Time-Dependent Quantum-Mechanical Approaches to the Continuous Spectrum: Scattering Resonances in a Finite Box

AUDREY DELL HAMMERICH, J. GONZALO MUGA AND RONNIE KOSLOFF*
Department of Physical Chemistry and The Fritz Haber Research Center for Molecular Dynamics, The Hebrew University of Jerusalem, Jerusalem 91904, Israel

(*Received 5 April 1989*)

Abstract. Several novel aspects of scattering resonances are studied. An expression, valid for a finite box, relating the continuum phase shift with the energy shift and unperturbed level separation is proposed and applied to obtain the resonance parameters. The effect of the resonance on propagating a wavepacket in imaginary time is studied. It is observed that the resonance strongly affects the cumulants of the energy distribution. In particular, a local minimum of the first derivative of the energy with respect to time (proportional to the second cumulant) serves to estimate the resonance energy and wavefunction. Once the estimate is known, the autocorrelation function is used to evaluate the resonance width. Alternatively, a new iterative approach is developed that is capable of selectively yielding an arbitrary band of energy eigenvalues and eigenfunctions on a grid. This method is applied to give those energy levels that are of interest for the discrete computation of the resonant phase shift, i.e., those close to resonance. Exact (analytical) and approximate results are in good agreement for a particular separable potential model in one dimension. These methods can be extended to realistic potentials in higher dimensions.

1. INTRODUCTION

Resonance phenomena arise in many areas of chemistry and physics. Their characterization is not, however, uniquely given. As a caveat to Howland's Razor[1] "No satisfactory definition of a resonance can depend only on the structure of a single operator on an abstract Hilbert space," we would like to add "nor on a single numerical calculation." In this article, we wish to emphasize some new aspects of scattering resonances, namely the capability of determining resonance parameters through a box discretization of the phase shift and through a time-dependent framework.

Time-dependent quantum-mechanical methods have emerged as one of the major tools for describing and simulating molecular dynamics.[2] When implementing the time-dependent approach upon a grid, a box normalization is usually implied. This can severely restrict the general applicability of grid methods for probing the continuous spectrum and the embedded resonance states. In particular, it is not obvious how typically continuum quantities like resonance energies and lifetimes can be obtained nor how they will be affected by a finite box normalization. The ability to bridge the gap between discrete and continuous representations is a challenge.

The transition from the discrete to the continuous spectrum has been repeatedly studied for both its intrinsic conceptual interest and its applications in quantum and statistical mechanics.[3-5] A major focus is an understanding of the relation between continuum quantities and those of the corresponding discrete spectrum. Some aspects of this relation have already been explored in connection with scattering resonances.[4] Here an alternative view is given.

One of the main and older results,[3a]

$$\eta(E) = -\lim \frac{\Delta(E)}{\delta(E)} , \qquad (1.1)$$

equates the continuum phase shift at a given energy to the ratio of two discrete spectral quantities, the perturbed level shift, Δ, and the free level separation, δ. This relation was first derived for partial waves with local and spherically symmetric potentials and in the limit of an infinite normalization box. (It has been

*Author to whom correspondence should be addressed.

proven, however, to be valid in more general cases.[3b,5]) Clearly though, an infinite box cannot be implemented upon a grid. In order to relax this limitation, we have generalized Eq. (1.1). The new expression (see Eq. (2.13) below) is valid under less restrictive conditions (for the particular model potential used here, the box is large enough so that terms exponentially decreasing with the length of the box can be neglected), enabling us to obtain the value of the continuum phase shift at the energies of the perturbed discrete box levels. This information can then be used to calculate resonant energies and lifetimes by comparison with parametrized expressions for the phase shift near resonance.

In this approach, the position of the perturbed energy levels is a necessary input. While there are several numerical procedures for determining the energy levels, the dynamical grid methods are a natural choice as the finite box size is explicitly incorporated. Here a relaxation method is chosen,[6] since it directly provides both the eigenvalue spectrum and the corresponding wavefunctions. Hence, a direct comparison with the exact continuum stationary scattering states can be made to determine whether the discrete "resonant" eigenfunctions keep the main feature of the continuum resonant states, namely their spatial localization in the interaction region. Moreover, by directing attention to the energy and its moments during relaxation, we shall be able to give another independent estimate for the resonance energy and an approximate form for the wavefunction. This approximate wavefunction can then be propagated in real time, employing a complex optical potential[7] to obtain its autocorrelation function and, thereby, also another independent estimate for the resonance width.

As an initial probe of our generalization of Eq. (1.1) and of the viability of discrete time-dependent methods in characterizing resonance states, a model separable potential, for which analytical results are known,[5,8] will be used.

The article is organized as follows: Section 2 describes the model and generalizes Eq. (1.1), Section 3 provides a review of the relaxation methods, Section 4 compares exact with approximate results, and Section 5 concludes with a discussion.

2. THE SEPARABLE POTENTIAL

A model separable potential, $\hat{V} = |\chi\rangle V_0 \langle\chi|$, will be used to compare exact with approximate results. For a particular choice of χ,[8]

$$\chi(x) = \left[\frac{a}{\hbar}\right]^{1/2} \exp(-a|x|/\hbar) \tag{2.1}$$

$$\chi(p) = \left[\frac{2a^3}{\pi}\right]^{1/2} \frac{1}{a^2 + p^2} ,$$

all the quantities of interest, resonance energies, lifetimes, phase shifts, etc., are known analytically.[5] Note the normalization, $\langle\chi|\chi\rangle = 1$. In the basis set diagonalizing the $\hat{S}$ matrix, there are two eigenstates of the Hamiltonian for any given positive energy E_p. One of them is the antisymmetric combination of plane waves:

$$\frac{1}{2^{1/2}}[\exp(ipx/\hbar) - \exp(-ipx/\hbar)]. \tag{2.2}$$

These functions are also eigenstates of $\hat{H}_0$ and do not experience the potential. The corresponding $\hat{S}$ matrix elements are equal to one, and the phase shift vanishes. In the symmetric subspace, matrix elements for the $\hat{S}$ matrix and the phase shift η are given by:[5]

$$S = \frac{X - iY}{X + iY} \tag{2.3}$$

$$\eta = -\operatorname{arccot}(X/Y) \tag{2.4}$$

where we have used the dimensionless variables:

$$X = |P|[(P^2 + 1)^2 + 2v(P^2 + 3)] \qquad Y = 4v \tag{2.5}$$

with $P = p/a$ and $v = V_0 m/a^2$. The reflectance coefficient,[8]

$$R = \frac{Y^2}{X^2 + Y^2} , \tag{2.6}$$

has in general two peaks, one being at zero energy (see Ref. 5 for details). Only the other peak can be associated with a resonance in the sense that one finds, besides the maximum of R, a sharp increase of the phase shift, a pole of the $\hat{S}$ matrix, and an excess density in the potential region. The resonance peak is located at $P^2 = v - 1 + \sqrt{v^2 + 4v}$ for $v \geq 1/6$.

In the discrete, finite box version of the model, where periodic boundary conditions are imposed at $\pm L/2$, the allowed momenta are given by:

$$P_n = \frac{2\pi n}{l} , \quad n = 0, \pm 1, \ldots ; \quad l = \frac{La}{\hbar} . \tag{2.7}$$

One should distinguish between the two normalized possibilities for the χ wavefunction in the potential. If the coordinate representation is chosen, then

$$\tilde{\chi}_L(x) = \left[\frac{a}{\hbar}\right]^{1/2} \tilde{N}_L \exp(-a|x|/\hbar), \tag{2.8}$$

while for the momentum representation

$$\chi_L(p) = \left[\frac{4a^3\hbar}{L}\right]^{1/2} \frac{N_L}{a^2 + p^2} \tag{2.9}$$

which indeed correspond to different potentials. (They do not exactly form a discrete Fourier transform pair.) However, the differences vanish exponentially with l. Here the latter representation is chosen as it admits a simpler treatment.

The eigenvalues are the solutions of the equation $Q_0(z, L) = 1/V_0$, where

$$Q_0(z, L) = \langle \chi_L | \frac{1}{z - \hat{\mathbf{H}}_0} | \chi_L \rangle. \tag{2.10}$$

After evaluating this matrix element, the eigenvalue condition takes the form[5] (P is considered positive in the following):

$$\frac{V}{P(P^2+1)}\left[\frac{-lP(P^2+1)}{\sin^2(il/2)} + 2iP\cot(il/2)(P^2+3) + 4\cot(Pl/2)\right] N_L^2 = 1, \tag{2.11}$$

where it is assumed that positive eigenvalues are to be determined. Neglecting terms which decrease exponentially with l, the above equation reduces to:

$$\frac{2V}{P(P^2+1)^2}[3P + P^3 + 2\cot(Pl/2)] = 1, \tag{2.12}$$

and setting $P = P^0 + \gamma$, where P^0 is the value of the momentum satisfying the periodic boundary condition corresponding to the unperturbed level, Eq. (2.7), we obtain from the last equation and from Eq. (2.4)

$$\eta(P) = -\gamma\frac{l}{2}. \tag{2.13}$$

This is our fundamental result. It relates the continuum phase shift with the shift between the momenta of the free and the perturbed states. Equation (1.1) can be recovered by assuming that γ is small with respect to P^0 (this is even the case at low energies when the box is sufficiently large). Then P can be written as

$$P = P^0 + \frac{m\Delta}{P^0 a^2} \tag{2.14}$$

which, when substituted into $\cot(Pl/2)$, yields Eq. (1.1), Δ being the energy level shift and δ the free level separation

$$\delta = \frac{ph}{mL}. \tag{2.15}$$

Note that strictly speaking δ is the true energy level only when L is very large, since the exact expression is $\delta_{\text{exact}} = (ph/mL) + (h^2/2mL^2)$. The difference between Eq. (1.1) and Eq. (2.13) was of course unimportant in the original derivation of Eq. (1.1) for partial wave scattering[5a] since the limit $L \to \infty$ was formally taken. However, for our intended application at a finite L, Eq. (2.13) is clearly superior (the extension to partial waves and local potentials can be done according to Ref. 5a), since it involves fewer approximations.

For the practical use of Eq. (2.13) at finite l, the eigenvalues have to be found independently. For this particular model, Eq. (2.11) provides a graphical solution, the eigenvalues being given by the intersection of $y = Q_0 V_0$ with $y = 1$. The slope at these points also indicates the overlap between the potential and the eigenstates (large overlaps occur at the resonance energies):

$$-\left[\frac{\partial V_0 Q_0(z, L)}{\partial z}\right]^{-1}_{z=E} = \langle \Psi_E | \hat{\mathbf{V}} | \Psi_E \rangle. \tag{2.16}$$

In the graphical solution, we thus have two indicators of the resonance energy. One is a rapid change in the difference between the free and the perturbed levels relative to the free level separation, and the other the slope of the function $Q_0 V_0$ (see Fig. 1). But for a general potential scattering problem, such a graphical solution need not exist, and an efficient method for determining the eigenvalues must be employed.

3. THE RELAXATION METHODS

Conventionally, eigenvalues and eigenfunctions are obtained by expanding the state of the system in a large basis set and subsequently diagonalizing the Hamiltonian matrix in this set, a procedure limited only by the size of the basis set expansion.[9] Introduction of the Fourier transform of the long-time propagated autocorrelation function of the initial state, with the propagated wavefunction[10]

$$\tilde{F}(E) = \int_{-\infty}^{+\infty} \exp(iEt/\hbar)\langle \Psi(0) | \Psi(t) \rangle dt = \sum_n |a_n|^2 \delta(E - E_n), \tag{3.1}$$

demonstrated the utility of grid methods for obtaining the spectrum of eigenvalues. The corresponding eigenfunctions can be recovered by a numerical Fourier transform of the propagated wavefunction at the calculated energy eigenvalues. An alternative procedure based upon a direct relaxation method on a grid (a propagation in imaginary time) has proved to be very efficient.[6] As this procedure and several variants are employed here, they will be briefly described.

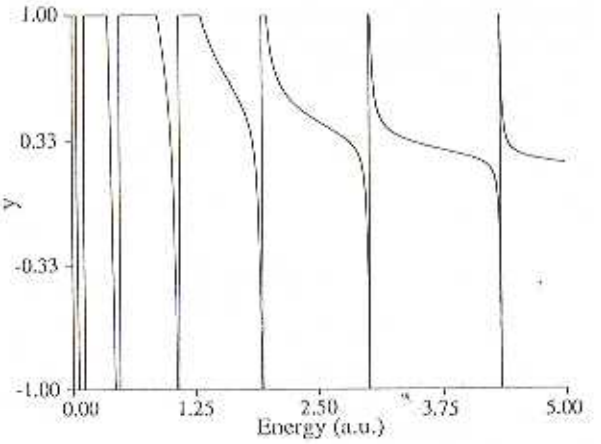

Fig. 1. The function represented is given by $y = Q_0V_0$ for $|Q_0V_0| \leq 1$, $y = 1$ for $Q_0V_0 \geq 1$, and $y = -1$ for $Q_0V_0 \leq -1$ for the case $V_0 = m = a = 1$. The 13 energies in the interval $0 \leq E \leq 5$ satisfying $Q_0V_0 = 1$ are eigenvalues of the Schrödinger equation (the first four starting from the right actually seem to coalesce into two). Two types of eigenvalues can be distinguished. From the origin (which is not an eigenvalue of $\hat{\mathbf{H}}$), the even eigenvalues are also solutions of the unperturbed Hamiltonian. Their separation, δ, is the free level separation. The level shift, Δ, is given by the separation between a given free level and the next neighbor eigenvalue on the right (the level shifts are represented by solid lines at $y = 1$). Note the clear decrease of the quantity δ/Δ at resonance (see also Fig. 2a).

Denoting the eigenvectors of $\hat{\mathbf{H}}$ by ϕ_n, an initial estimate for the wavefunction can formally be considered to be expanded in this set

$$\Psi(0) = \sum_n a_n \phi_n, \tag{3.2}$$

where normalization of Ψ determines the expansion coefficients, $a_n = \langle \phi_n \,|\, \Psi(0) \rangle$. The time evolution of Ψ is then given by

$$\begin{aligned} \Psi(t) &= \exp(-i\hat{\mathbf{H}}t/\hbar)\Psi(0) \\ &= \sum_n a_n \exp(-iE_n t/\hbar)\phi_n. \end{aligned} \tag{3.3}$$

Consider now an imaginary time propagation where $\tau = it/\hbar$,

$$\Psi(\tau) = \sum_n a_n \exp(-E_n\tau)\phi_n. \tag{3.4}$$

Since normalization is lost during this relaxation,

$$\langle \Psi(\tau) \,|\, \Psi(\tau) \rangle = \sum_n |a_n|^2 \exp(-2E_n\tau), \tag{3.5}$$

the normalized wavefunction is given by

$$\Psi(\tau) = \frac{\sum_n a_n \exp(-E_n\tau)\phi_n}{\left[\sum_n |a_n|^2 \exp(-2E_n\tau)\right]^{1/2}}, \tag{3.6}$$

and $\Psi(\tau)$ will henceforth denote this normalized form. In addition, energy is not strictly conserved:

$$\begin{aligned} \langle E(\tau) \rangle &= \langle \Psi(\tau) \,|\, \hat{\mathbf{H}} \,|\, \Psi(\tau) \rangle \\ &= \frac{\sum_n |a_n|^2 E_n \exp(-2E_n\tau)}{\sum_n |a_n|^2 \exp(-2E_n\tau)}. \end{aligned} \tag{3.7}$$

From Eq. (3.4) one finds that the contribution from each eigenfunction relaxes to zero at a rate proportional to its eigenvalue. Since the ground state relaxes most slowly, its contribution to the expansion persists beyond the time when the higher eigenvalue terms have effectively decayed. Once found, the ground state is projected out of the Hilbert space. This procedure is repeated until the desired wavefunctions are obtained.

One cannot fail to remark on the formal similarity between Eq. (3.7) and a canonically averaged energy, with the denominator of Eq. (3.7) assuming the role of a partition function, the $|a_n|^2$, degeneracy factors, and 2τ identified with $\beta(1/kT)$. In fact, consistency can be shown by "working out" the thermodynamic connection.[11] For instance, from the dependence of the average energy upon β (see Eq. (3.8) below), one finds that $\langle E \rangle$ is a decreasing function of β, a result completely in accord with the decay of the higher eigenvalue terms over the ground state during the relaxation process.

We shall variously adapt this relaxation method. Firstly, so that it is capable of giving an estimate of the continuum resonance energy and a wavepacket strongly overlapping with the resonant states, without the need to sequentially determine the wavefunctions of the intermediate states. Monitoring the autocorrelation function of this wavepacket allows a determination of its lifetime. A second modification employs the resonance energy estimate in an algorithm that will converge to the box eigenvalues (and eigenfunctions) of interest.

One of the dominant attributes of a resonance is a localization of its wavefunction in the potential region. In addition to this localization of the exact resonance state (which here is understood as the continuum eigenstate at the resonance energy), nearby continuum eigenstates are also perturbed by the potential so their wavefunctions, too, have enhanced localizations in the interaction region and contribute to the resonance width. Then, if an initial state were chosen which

overlapped significantly with the localized eigenstates, its formal expansion (Eq. (3.2)) would have dominant contributions from this "width." Hence, one would anticipate that the relaxation behavior of this initial state would reflect the existence of the resonance.

The foundation for these ideas may be more concretely examined by returning to Eq. (3.7) and ascertaining the behavior of the relaxed energy as a function of τ. The first derivative,

$$\frac{\partial\langle E\rangle}{\partial\tau} = -2\langle(E-\langle E\rangle)^2\rangle = -2\sigma_E^2, \qquad (3.8)$$

is simply a factor of the variance of the energy (the second energy cumulant) and a measure of the dispersion in energy values, where the relaxation time-dependent probability for the nth level is given by

$$P_n = \frac{|a_n|^2\exp(-2E_n\tau)}{\sum_n |a_n|^2\exp(-2E_n\tau)}. \qquad (3.9)$$

If the above probability distribution were a Gaussian in E_n, then its width would be σ_E. However, it is inappropriate in general to make such a Gaussian approximation. Our distribution is over a weighted set (via the expansion coefficients) of eigenstates and, though it may be peaked at the resonance energy for suitably chosen initial states and values of τ, this is not an a priori fact. But additional information on the distribution is available from the second time derivative:

$$\frac{\partial^2\langle E\rangle}{\partial\tau^2} = 4\langle(E-\langle E\rangle)^3\rangle. \qquad (3.10)$$

The quantity in brackets (the third cumulant) characterizes the degree of asymmetry (or skewness) of the distribution where a positive value indicates a positive asymmetric tail and a negative value the converse. If the resonances are well separated and the initial energy is above the first resonance, the initial distribution will be skewed to higher energies. As the relaxation progresses, the exponential factor in Eq. (3.9) will compensate this asymmetry until the second derivative vanishes, close to the resonance energy.

As to be expected, the fourth moment of the time-dependent distribution is related to the third partial derivative:

$$\frac{\partial^3\langle E\rangle}{\partial\tau^3} = -8[\langle(E-\langle E\rangle)^4\rangle - 3\sigma_E^4]. \qquad (3.11)$$

Here the terms in brackets are commonly referred to as the kurtosis of the distribution (the fourth cumulant) with positive values indicating a peaked distribution and negative values a flat one. The above expressions can easily be derived from the derivative of the moments,

$$\frac{\partial\langle E^n\rangle}{\partial\tau} = -2(\langle E^{n+1}\rangle - \langle E\rangle\langle E^n\rangle), \qquad (3.12)$$

and are perhaps even more familiar if recognized as being cumulants[12] of the energy distribution.

An initial state that overlaps well with the potential region and has an initial energy above the resonance value can be propagated in imaginary time until the point where its underlying distribution becomes symmetrical (Eq. (3.8) displaying a local maximum and Eq. (3.10) vanishing) and is peaked about the resonance energy (Eq. (3.11) negative). At this point, the real time behavior of this relaxed wavefunction, $\Psi_r(0)$, is monitored. The time dependence of the wavefunction is determined by propagating in time via a Chebychev polynomial expansion of the evolution operator[13] using a complex optical potential.[7] The imaginary potential provides an absorbing boundary, thereby allowing simulation of evolution in the continuum rather than in the periodic boundary conditions of the box. From its autocorrelation function, the lifetime τ_r may be deduced:[14]

$$|\langle\Psi_r(0)\,|\,\Psi_r(t)\rangle|^2 \approx \exp(-t/\tau_r). \qquad (3.13)$$

Alternatively, or even in addition to the lifetime, the imaginary time behavior of $\Psi_r(0)$ can be monitored. Since an initial estimate is quickly forthcoming for the resonant energy in the modified relaxation procedure, an algorithm that will determine just those energy levels which are relevant for the resonance of interest is highly desirable. Once the estimate z is known, a new imaginary time propagation is proposed,

$$\Psi(\tau) = \exp[-\tau(\hat{\mathbf{H}}-z)^m]\Psi_r(0) = \sum_n a_n\exp[-\tau(E_n-z)^m]\phi_n, \qquad (3.14)$$

where m is an even integer, which converges to the eigenstate whose eigenvalue lies closest to z. Additional levels to be used in Eq. (2.13) can be calculated by equating z to nearby unperturbed energies. We have already achieved the desired convergence for cases where $m = 2$.

Since this is a new propagation, a brief description of its implementation is warranted. The method is based upon propagating the time-dependent Schrödinger equation by a polynomial expansion of the evolution operator $\hat{\mathbf{U}} = \exp(-i\hat{\mathbf{O}}t/\hbar)$ where the real time propagation is converted into an imaginary one, $\tau = it/\hbar$. We

have adapted the normal relaxation method ($\hat{O} = \hat{H}$)[6] by directly expanding the new propagator, $(\hat{H} - z)^m$, in a series of real Chebychev polynomials. As these polynomials are orthogonal on $[-1, 1]$, the domain of eigenvalues of the propagator must be renormalized and shifted:

$$\hat{H}^2_{norm} = \frac{2(\hat{H} - z\hat{I})^2 - \Delta E_z^2 \hat{I}}{\Delta E_z^2} \quad (3.15)$$

In order to assure compliance with the interval, the domain is "overestimated" by setting $\Delta E_z^2 = (K_{max} + V_{max})^2 + z^2$, with K_{max} and V_{max} being the maximum kinetic and potential energy, respectively, represented upon the grid. Then, the evolution of the wavefunction can be approximated as

$$\Psi(\tau) \approx \exp(-\Delta E_z^2 \tau/2) \sum_{n=0}^{N} a_n(\Delta E_z^2 \tau/2) T_n(-\hat{H}^2_{norm}) \Psi_r(0), \quad (3.16)$$

where T_n is the real Chebychev polynomial and a_n is an expansion coefficient.

Information on the distribution and the contributions from the underlying states may thus be found in the time dependence of the relaxed energy and, in particular, the resonance energy and width can be estimated as shown in the examples provided in Section 4.3.

4. RESULTS

4.1. The "Discretized" Phase Shift

In this subsection, we shall concentrate on the application of Eq. (2.13) to obtain the phase shift and the resonance parameters. Three cases have been chosen by varying the parameters defining the interaction, and each has been studied for two different box sizes. Even for the smallest box studied, the values of the exact and the approximate phase shift are in excellent agreement, as depicted in Fig. 2. The degree of accuracy obtained is perhaps surprising when comparing the potentials of Fig. 3 with the box sizes.

The resonance parameters, given in Table 1 (subscripts 3 to 5), have been calculated by fitting the points at the phase shift jump to the Breit–Wigner expression for the phase shift (E_3, Γ_3: two points, one above and one below $\eta = -\pi/2$ for $l = 12.8$; E_4, Γ_4: the same for $l = 25.6$; E_5, Γ_5: four points taken from the two box sizes):

$$\eta = \arctan\left[\frac{\Gamma/2}{E - E_R}\right]. \quad (4.1)$$

The largest deviation from the exact values (E_1 is the energy at the resonance maximum of R and Γ_1 is the width, at half height, of the peak of R, E_2 and $\Gamma_2/2$ are the real and imaginary parts of the resonance pole) corresponds to the case $v = 1$. This is not due to a failure in reproducing the phase shift, but to the fact that the Breit–Wigner parametrization is not accurate in this case. The reason is the existence of other poles of the $\hat{S}$ matrix that cannot be neglected here (a detailed analysis of this phenomenon has been given elsewhere[5]). For $v = 1$, the two peaks of the reflectance coefficient are highly coupled, and thus the halfwidth of the resonance peak cannot be properly defined ($\Gamma_1/2$). The comparison can, however, be made with the imaginary part of the resonant pole ($\Gamma_2/2$).

Table 1. Resonance Energies and Halfwidths Calculated for $v = 1$, $v = 4$, and $v = 8$

Parameter	$v = 1$ ($V_0 = m = a = 1$)	$v = 4$ ($V_0 = m = 1$; $a = 0.5$)	$v = 8$ ($V_0 = 8$; $m = a = 1$)
E_1	1.118	1.082	8.398
$\Gamma_1/2$	—	0.0644	0.1996
E_2	1.196	1.087	8.406
$\Gamma_2/2$	0.2702	0.0595	0.1988
E_3	1.070	1.065	8.386
$\Gamma_3/2$	0.3154	0.0664	0.2167
E_4	1.026	1.075	8.392
$\Gamma_4/2$	0.3134	0.0599	0.1895
E_5	1.059	1.070	8.406
$\Gamma_5/2$	0.3036	0.0644	0.2141
E_6	0.992, 0.996, 1.086	1.079, 1.028, 0.973	8.050, —, —
$\Gamma_6/2$	—	0.0649	0.244

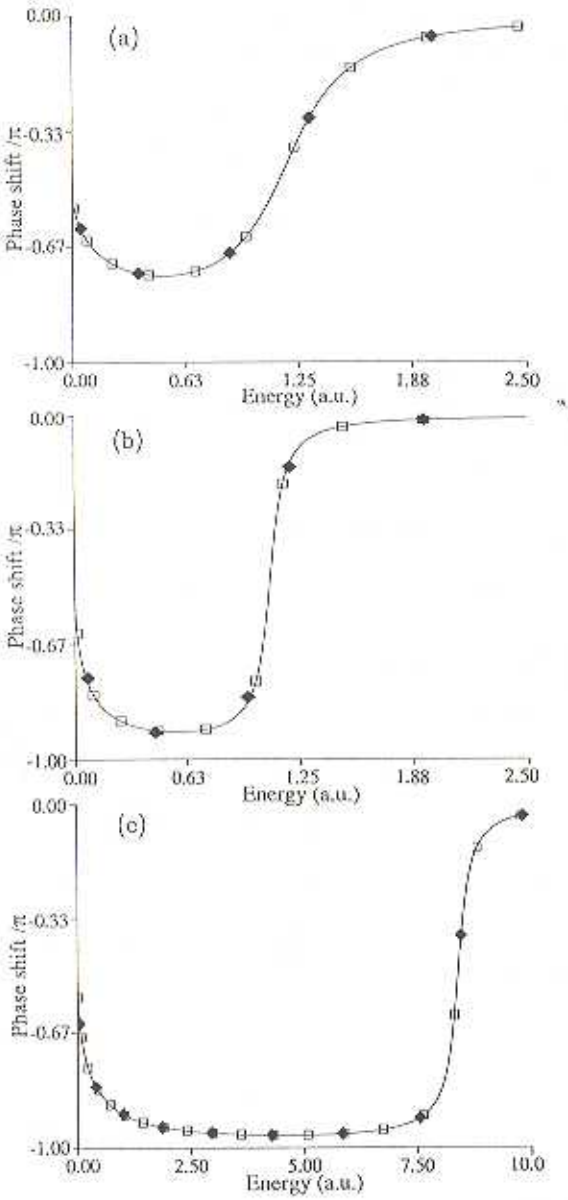

Fig. 2. The exact phase shift (in units of π) vs. energy, shown as a continuous line, for the cases $V_0 = m = a = 1$ (a), $V_0 = m = 1$, $a = 0.5$ (b), and $V_0 = 8$, $m = a = 1$ (c). The solid diamonds indicate the values obtained from Eq. (2.13) for $l = 12.8$, and the squares the values for $l = 25.6$.

Another point of interest is the comparison between the continuum resonance eigenstates and the box eigenstates close to the resonant energy (Fig. 3). Clearly, none of the box states reproduces the finer details of the continuum, but they still remain localized, and the main features can be distinguished by a proper linear combination.

4.2. The "Discretized" Eigenvalues and Wavefunctions

The positions of the perturbed energy levels were determined by the unmodified imaginary time relaxation procedure described in Section 3. Examples of the relaxed wavefunctions for the three cases examined are shown in Fig. 3 for the smaller box size. In addition to the box "resonant" state, i.e., the one with the larger overlap with the potential, the two adjacent eigenstates are also given. In all cases, the box "resonant" state overlaps well with the exact continuum stationary scattering state. The case of $v = 8$ (Fig. 3c) evidences a box size whose "resonant" eigenfunction greatly overlaps its continuum counterpart, with an overlap of 0.957, and is almost coincident with it. From Fig. 2, we see that this case has a phase shift lying closest (the solid diamonds denote the smaller box size) to the resonance value of $-\pi/2$.

4.3. Imaginary and Real Time Propagations for Resonance Widths

Modifying the relaxation procedure so that all of the intervening eigenstates need not be computed enables us to quickly obtain an estimate for the resonance energy as well as information on the nearby perturbed continuum states attributing to the "resonance width." By monitoring the cumulants of the energy distribution as a function of τ (derivable from Eqs. (3.8), (3.10), and (3.11)) of an initial state which overlaps with the potential, a Gaussian for example, the distribution is uniquely manifested. In the normal method for determining eigenvalues and eigenfunctions, relaxation proceeds until the ground state is obtained. The cumulant (variance) in Eq. (3.8) then merely exhibits a sum of exponential decays until the derivative vanishes, at which point the eigenfunction corresponding to the ground state is the only term left in Eq. (3.6). Without projecting out all of the lower eigenstates and choosing a semilocalized initial state like a Gaussian, the relaxation behavior is quite different. Figure 4 exhibits this behavior for initial states whose energies are 10% and 25% above the resonant value. For the time period examined, Fig. 4 shows that the initial distribution at zero time, though peaked, has the greatest asymmetry and a large variance. At the point of a local minimum in the variance, the distribution has evolved until it is still peaked but now symmetrical. Further evolution of the distribution continues until a local maximum in the variance is obtained. At this point,the energy-dependent probability distribution attains its most flattened state. The major differences between Fig. 4a and 4b are that the initial distribution has a larger positive tail and dispersion at 25% excess energy while at 10% the great-

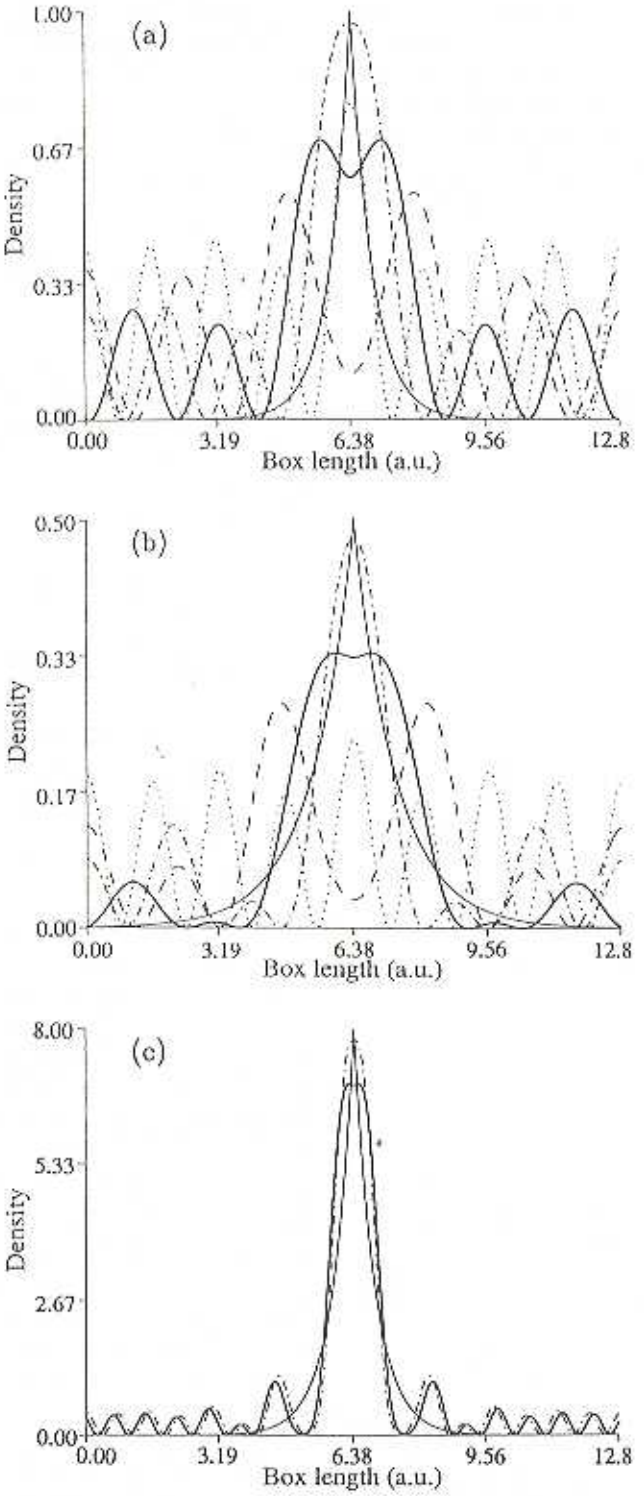

Fig. 3. Potential, box eigenfunctions, and continuum stationary scattering state for $l = 12.8$. Solid lines: light = potential, heavy = stationary state; dashed line: eigenfunction below box resonance; dash-dotted line: box resonance eigenfunction; dotted line: eigenfunction above box resonance. For the potential density, $V_0|\chi(x)|^2$ is plotted (see Eq. (2.1)). a. $v = 1$ with a factor of 3 for the wavefunctions. b. $v = 4$ with a factor of 1.2. c. $v = 8$ with a factor of 11 and omission of the off-resonance eigenfunctions for clarity.

est overall dispersion and flatness to the distribution is found (at 1.5 a.u.). These qualitative statements can be directly translated into a precise meaning since the probability distribution can be calculated from the known box eigenstates and the overlap of the initial wavepacket with each of these states via Eq. (3.6). Figure 5 shows the distributions for the initial state, dispersion minimum, and dispersion maximum corresponding to Fig. 4. The conclusions from Fig. 4 are exactly borne out in Fig. 5, especially with respect to the tails of the distribution and when a symmetrical state is achieved.

The ability to use in fact, rather than just formally as-

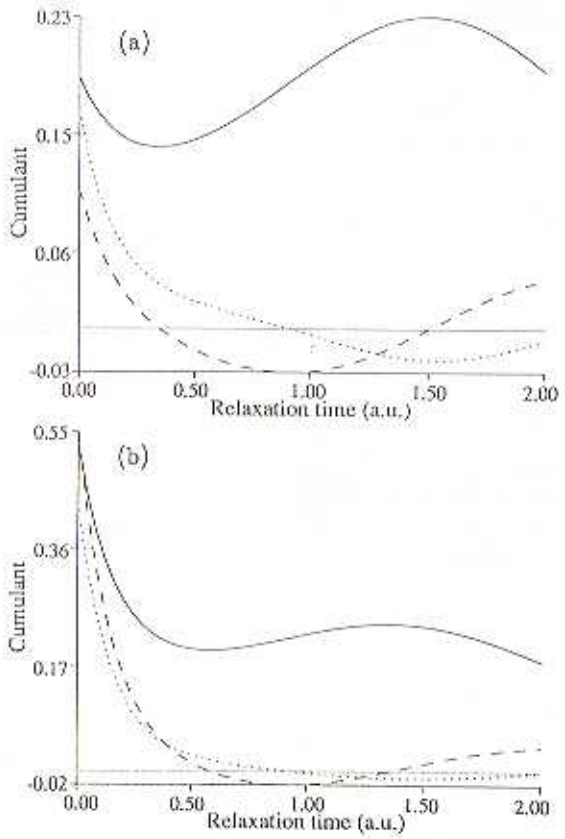

Fig. 4. Energy cumulants for $\nu = 4$ as a function of relaxation time. Solid curve: variance (second cumulant), Eq. (3.8)/(−2); dashed curve: skewness (third cumulant), Eq. (3.10)/8; dotted curve: kurtosis (fourth cumulant), Eq. (3.11)/(−32). a. Initial energy 10% above resonant value. b. Initial energy 25% above resonant value with dotted line cumulant reduced by an additional factor of 2. At the points where the dashed line passes through zero (light solid line), the distribution is separated into regions characterized by having a positive tail, a negative tail, and then again a positive tail, respectively. The point where the dotted line passes through zero delineates a peaked distribution from a flat one.

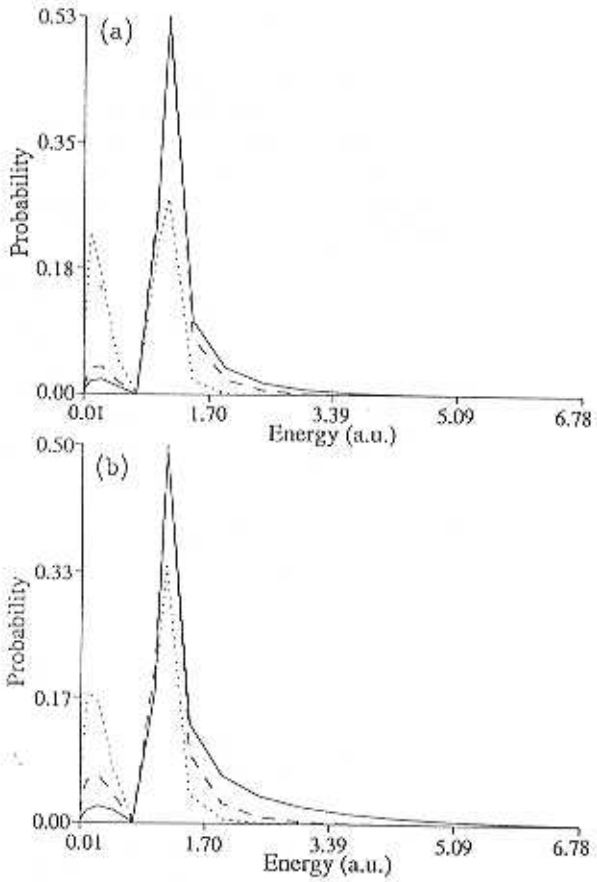

Fig. 5. Probability distribution as a function of energy for critical values of the cumulants for $\nu = 4$. Solid line: distribution for the initial state at $\tau = 0$; dashed line: distribution when variance exhibits a local minimum; and dotted line: distribution when variance attains a local maximum. Initial energy 10% (a) and 25% (b) above resonant value. Note more prominent high energy tail in Fig. 5b and the greater degree of bimodality in the dotted distribution of Fig. 5a.

presumed in Eq. (3.2), an expansion in box eigenstates with a known probability distribution allows us to show that the relaxation method can converge a wavepacket to a superposition dominated by the continuum resonant state and nearby perturbed states (this is true, as elaborated upon in the Discussion, since the resonance imposes a dynamics dominated by local properties in space), without the need to project out the lower states. The low energy tails in Fig. 5 show that these states comprise a negligible contribution. This being the case, the converged state should be amenable to a determination of its lifetime and therefore provide another estimate for the resonance width. Figure 6 portrays the autocorrelation function of Eq. (3.13) for the three cases considered here. For the cases $\nu = 4$ (Fig. 6a) and

$v = 8$ (Fig. 6c), a pure exponential decay with a single sinusoidal modulation is observed; two states are strongly interfering and "beating" with each other.[15] As the case of $v = 8$ gave a width approximately 20% higher than the analytic values, the autocorrelation function was also obtained for the box resonant state. Within the precision of our numerical analysis, the width was identical to that of the relaxed wavepacket. As discussed in Section 4.1, the case of $v = 1$ (Fig. 6a) is

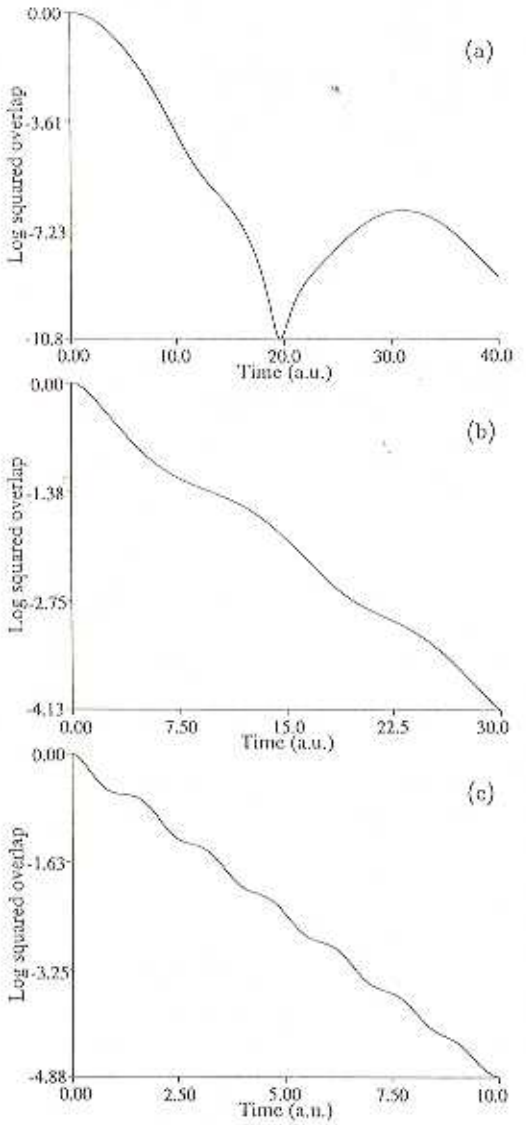

Fig. 6. Autocorrelation function (log of the squared overlap) as a function of time for the cases $v = 1$ (a), $v = 4$ (b), and $v = 8$ (c). Note that the latter two cases clearly exhibit a single sinusoidal modulation due to interference with the resonance state. In Fig. 6a, however, the modulation is large (the second recurrence is hardly visible) and evidences coupling of the resonance state with a long-lived minor component.

richer in structure due to the close proximity of more than one pole of the $\hat{S}$ matrix. Its autocorrelation function evidences a modulation upon a long-lived component. In Fig. 6, the beginning of the second recurrence is observed on the far end of its autocorrelation function.

The results of the various time propagations employed are summarized in Table 1. E_6 represents the estimate for the resonance energy obtained via the modified relaxation procedure for initial states that are 10%, 25%, and 50% above the resonant energy. These values are taken at the local minimum of the energy variance (Eq. (3.8)). The halfwidths, $\Gamma_6/6$, are from the time dependence of the autocorrelation function of an initial state taken at the variance minimum. Because of the presence of the low energy terms in the expansion (Eq. (3.6)), the relaxation estimate represents a lower bound to the true resonance energy. This is also to be expected for systems containing more than one resonance if they are well separated. The halfwidths are in good agreement with the analytic results.

5. DISCUSSION

We have emphasized the characterization of resonances through the box and time-dependent approaches. While the resolution of the method to determine the phase shift, i.e., the "density" of states per unit energy available, is enhanced by a large box size, the excellent agreement between approximate and exact phase shifts allows mixing of two or more box size results until the desired resolution is obtained. Although the model potential is one-dimensional, the methods employed are broadly applicable and do not suffer from this dimensionality limit. In particular, the relaxation procedure is routinely used in one, two, and three dimensions, and even an imaginary time propagation for six degrees of freedom has been accomplished on a minicomputer.[16] The generality of the schemes used means that they have application to other physical systems in addition to those containing resonances. For instance, the propagator of Eq. (3.16) can directly yield the eigenstate and eigenvalue for some arbitrarily specified level (dependent upon the value of z) of a bound system. A problem of current active interest, the highly excited levels of HCN, would be a good candidate.

As a final note in closing, we would like to return to the challenge of bridging the gap between the discrete and continuous representations and offer a resolution. In addition to directly bridging this gap (a nontrivial task), e.g., by the development of Eq. (2.13) equating the continuum phase shift to two discrete spectral quantities, our time-dependent methods have implic-

itly done so. To see how this is accomplished, we need to recall that quantization results when the wavefunction is subjected to the boundary conditions of the problem. Examining the wavefunctions of Fig. 3, the heavy solid line does not satisfy the periodic boundary conditions of the box, while the dashed, dotted, and dash-dotted lines define wavefunctions which do. The former represents the exact continuum stationary scattering state (boundaries at $-\infty$ and $+\infty$), while the latter three are eigenfunctions of the box with periodic boundary conditions imposed at $-L/2$ and $+L/2$. How can one simulate a propagation that satisfies continuum boundary conditions in a discrete calculation upon a grid? This work presents two ways of doing so. Use of a complex optical potential eliminates the periodic boundary conditions of the box. Then, the time evolution of a wavefunction initially localized in the potential region is the continuum evolution, at least within the region where the imaginary potential is not applied. These are the conditions under which the autocorrelation function (Eq. (3.13)) and hence the resonance width were obtained. In addition to explicitly changing the boundary conditions of the Hamiltonian, one can localize the wavefunction so that it has negligible amplitude in the boundary region. The choice of a Gaussian wavepacket yields a semilocalized function both in coordinate space and in momentum space. Although this function cannot be strictly confined to a finite volume (e.g., the potential region), the amplitude out of a volume in phase space exponentially converges to zero with an increase in volume.[2] This is a well-known property of a Gaussian distribution which we may restate in the terminology of probability: 99.74% of the distribution is to be found within 3σ of its mean. Hence, if we center a Gaussian wavepacket about the potential and choose a box size sufficiently greater than 3σ, we have a wavefunction which does not "feel" a periodic potential but rather the potential of the continuum. A similar argument would apply to momentum space. The concept that a confined function in phase space can be discretely represented with no loss of either information or accuracy finds its formal justification in the Whittaker–Kotel'nikov–Shannon sampling theorem.[17] This is the underlying basis of our modified relaxation method for obtaining an estimate for the resonance energy and a wavepacket converged to a superposition dominated by the continuum resonant state and nearby perturbed states.

"Adiabatic" molecules that contain resonance states even though their potential energy surfaces exhibit no wells are interesting systems that may demonstrate the applicability of our methods. Finding these dynamic resonances in reactive scattering problems and determining the energy dependence of the phase shift and width are natural problems for this approach.

Acknowledgments. The Fritz Haber Research Center for Molecular Dynamics is supported by the Minerva Gesellschaft für die Forschung, Federal Republic of Germany. A.D.H. gratefully acknowledges receipt of a Lady Davis postdoctoral fellowship and J.G.M. thanks Volkswagen Stiftung for support.

REFERENCES

(1) (a) Howland, J. *Pac. J. Math.*, 1974, **55**: 157. (b) Howland, J. *Bull. Am. Math. Soc.*, 1978, **78**: 380. (c) Simon, B. *Int. J. Quantum Chem.*, 1978, **14**: 529.
(2) Kosloff, R. *J. Phys. Chem.*, 1988, **92**: 2087.
(3) (a) Fukuda, N.; Newton, R.G. *Phys. Rev.*, 1956, **103**: 1558. (b) deWitt, B.S. *Phys. Rev.*, 1956, **103**: 1565. (c) Goldberger, M.L. *Phys. Fluids*, 1959, **2**: 252. (d) Kohn, W.; Majumdar, C. *Phys. Rev.*, 1965, **A138**: 1617.
(4) (a) Hazi, A.U.; Taylor, H.S. *Phys. Rev.*, 1970, **A1**: 1109. (b) Truhlar, D.G. *Chem. Phys. Lett.*, 1974, **26**: 377. (c) Maier, C.H.; Cederbaum, L.S.; Domcke, W. *J. Phys. B*, 1980, **13**: L119. (d) Lefebvre, R. *J. Phys. Chem.*, 1985, **89**: 4201. (e) Rittby, M.; Elander, N.; Brandas, E. *Mol. Phys.*, 1982, **45**: 553. (f) Macias, A.; Martin, F.; Riera, A.; Yáñez, M. *Int. J. Quantum Chem.*, 1988, **33**: 279.
(5) Muga, J.G.; Snider, R.F.; to be published.
(6) Kosloff, R.; Tal-Ezer, H. *Chem. Phys. Lett.*, 1986, **127**: 223.
(7) Kosloff, R.; Kosloff, D. *J. Comput. Phys.*, 1986, **63**: 363.
(8) Snider, R.F. *J. Chem. Phys.*, 1988, **88**: 6438.
(9) Noid, D.W.; Marcus, D. *J. Chem. Phys.*, 1979, **67**: 3383.
(10) Feit, M.D.; Fleck, J.A.; Steiger, A. *J. Comput. Phys.*, 1982, **47**: 412.
(11) Reiss, H.; Hammerich, A.D.; Montroll, E.W. *J. Stat. Phys.*, 1986, **42**: 647.
(12) Kubo, R. *J. Phys. Soc. Jpn.*, 1962, **17**: 1100.
(13) Tal-Ezer, H.; Kosloff, R. *J. Chem. Phys.*, 1984, **81**: 3967.
(14) Bisseling, R.H.; Kosloff, R.; Manz, J. *J. Chem. Phys.*, 1985, **83**: 993.
(15) Fano, U. *Phys. Rev.*, 1961, **124**: 1866.
(16) Bisseling, R.H.; Kosloff, R. *J. Comput. Phys.*, 1988, **76**: 243.
(17) (a) Whittaker, E.T. *Proc. R. Soc. Edinburgh*, 1915, **35**: 181. (b) Nyquist, H. *Trans. AIEE*, 1928, **47**: 617. (c) Shannon, C.E. *Proc. IRE*, 1949, **37**: 10.